

Instantaneous frequency and wave shape functions (I)

Hau-tieng Wu

Department of Mathematics, Princeton University, Fine Hall, Washington Road, Princeton NJ 08544-1000 USA.

Abstract

Although one can formulate an intuitive notion of instantaneous frequency, generalizing "frequency" as we understand it in e.g. the Fourier transform, a rigorous mathematical definition is lacking. In this paper, we consider a class of functions composed of waveforms that repeat nearly periodically, and for which the instantaneous frequency can be given a rigorous meaning. We shown that Synchrosqueezing can be used to determine the instantaneous frequency of functions in this class, even if the waveform is not harmonic, thus generalizing earlier results for cosine wave functions. We also provide real-life examples and discuss the advantages, for these examples, of considering such non-harmonic waveforms.

Keywords: Instantaneous frequency, wave shape function, Synchrosqueezing transform

1. Introduction

The term "instantaneous frequency" is somewhat of an oxymoron. In many cases, researchers who seek to decompose signals into different components, and who want to determine the "instantaneous frequency" of each, really seek to solve problems of the following form:

given a function of the form

$$f(t) = \sum_{k=1}^K A_k(t) \cos(2\pi\phi_k(t)), \text{ with } A_k(t), \phi'_k(t) > 0 \forall t, \quad (1)$$

compute $A_k(t)$ and $\phi'_k(t)$ and/or describe their properties.

The Synchrosqueezing transform, originally introduced in the context of audio signal analysis [5], and further analyzed in [4, 13], provides a way to determine $A_k(t)$ and $\phi'_k(t)$ uniquely, up to some pre-assigned accuracy, under some conditions on $f(t)$.

For some applications, decompositions of the form (1) are too restrictive. Consider, for instance, the function f illustrated in the left plot of Figure 1(a); it is a toy example of the type

$$f(t) = A(t)s(2\pi\phi(t)) \quad (2)$$

where, as before, $A(t)$ and $\phi'(t)$ vary slowly, and s is now no longer a cosine, but the periodic extension of the function in the right plot of Figure 1(a). It is clear that this $f(t)$ can be decomposed as in (1), simply by replacing s by its Fourier expansion; however, the representation (2) is much more efficient because it uses fewer terms. Another way in which one could reduce $f(t)$ to an expansion of type (1), with a *single* term, would be to "absorb" some of the properties of s into a modified phase function $m(t) := \cos^{-1}(s(2\pi\phi(t)))$.

Email address: hauwu@math.princeton.edu (Hau-tieng Wu)

This is the preferred solution in [8], where $m(t)$ is then called the “intra-wave” modulation, indicative of the nonlinear nature of the wave process generating $f(t)$. Although this would work for the example in Figure 1(a), it is not always possible to do this. Consider the function f in the left plot of Figure 1(b), clearly of the same type as in Figure 1(a); one would expect that the same remarks apply to both examples. However, because s has several maxima, it can not be written as $\cos(m(t))$, with m a monotonic mapping on $[0, 2\pi]$. A single-term expansion of type (1) can thus not deal with this example by using only “intra-wave modulation”. To nevertheless still reduce $f(t)$ to an expansion of type (1) with a single term, one can, instead, attempt to “absorb” some of the properties of s into a modified amplitude \tilde{A} . In this particular case,

$$s(t) = \left[\cos(0.8 \cos(t)) - \frac{\sin(t)}{\cos(t)} \sin(0.8 \cos(t)) - 1.4 \cos_+(t + 1/6)^2 \right] \cos(t) := w(t) \cos(t), \quad (3)$$

where $\cos_+(t) = \max\{0, \cos(t)\}$. So one can write $f(t) = \tilde{A}(t) \cos(2\pi\phi(t))$, with $\tilde{A}(t) = w(2\pi\phi(t))A(t)$. Note that this amplitude \tilde{A} varies much faster than A , masking the only slowly changing wave-pattern of $f(t)$. Even this solution is not always applicable. Consider the function f plotted on the left of Figure 1(c). Absorbing the “extraneous” extrema of the basic wave-pattern into a special \tilde{A} would lead to an amplitude that is no longer always positive, clearly an undesirable trait.

Although the examples in Figure 1 are just toy examples, similar phenomena can be observed in real-life signals, for example, in electrocardiography (ECG) (see Figure 2). As we shall see below, it is important, in these real-life examples, to tease apart the characteristics of the “shape” $s(t)$ from the slow variations in $\phi'(t)$ and $A(t)$. Rather than insisting on a representation of type (1), we are therefore, in this paper, interested in decompositions of the type

$$f(t) = \sum_{k=1}^K A_k(t) s_k(2\pi\phi_k(t)), \quad (4)$$

where we shall give the name “wave-shape function” (or, shorter, “shape function”) to the 2π periodic functions s_k , generalizing the cosine functions of (1) and [4], and where we assume that $|A'_k(t)|$ and $|\phi''_k(t)|$ are small compared with $\phi'_k(t)$, as in [4]. Functions of type (4) can be found in many applications. We already mentioned ECG signals; another medical signal of this same form is respiration.

The additional layer of generality in (4), when compared to (1), adds to the complexity of determining desirable decompositions of type (4) for a (noisy) signal f . Even for decompositions of type (1), uniqueness is not guaranteed (see e.g. [4]); this absence of uniqueness can obviously be only more pronounced for decompositions of type (4). Even when the decomposition is unambiguous, the algorithmic task will necessarily be more complex, since not only the $A_k(t)$ and $\phi_k(t)$, but also the $s_k(t)$ need to be determined, in general. We shall concentrate here on the determination of the amplitudes $A_k(t)$ and the instantaneous frequencies $\phi'_k(t)$ for the more generalized expansions (4), when the wave shape functions s_k are unknown; the determination of the wave shapes s_k themselves will be discussed in a later paper.

The main result of this paper is that, under the same technical conditions as in [4] (the ϕ'_k have to be sufficiently separated), we can determine $A_k(t)$ and $\phi'_k(t)$ via Synchrosqueezing, for suitable wave forms s_k . We shall apply this method to ECG and respiration signals, and show the clinical potential of the results. In the next section, we first discuss some properties of these signals in more detail. Section 3 states and proves the related theorems for two important cases: when f is essentially given by a single term, as in (2), with a lowest Fourier mode that is “not too small”, or when f is a sum of several waveforms, as in (4), with each s_k fairly close to a standard sine or cosine.

2. Two biomedical signals

The ECG signal can be measured easily and cheaply, and its clinical usefulness is well established. It is commonly accepted to model the ECG signal as a current dipole vector undergoing a periodic motion in

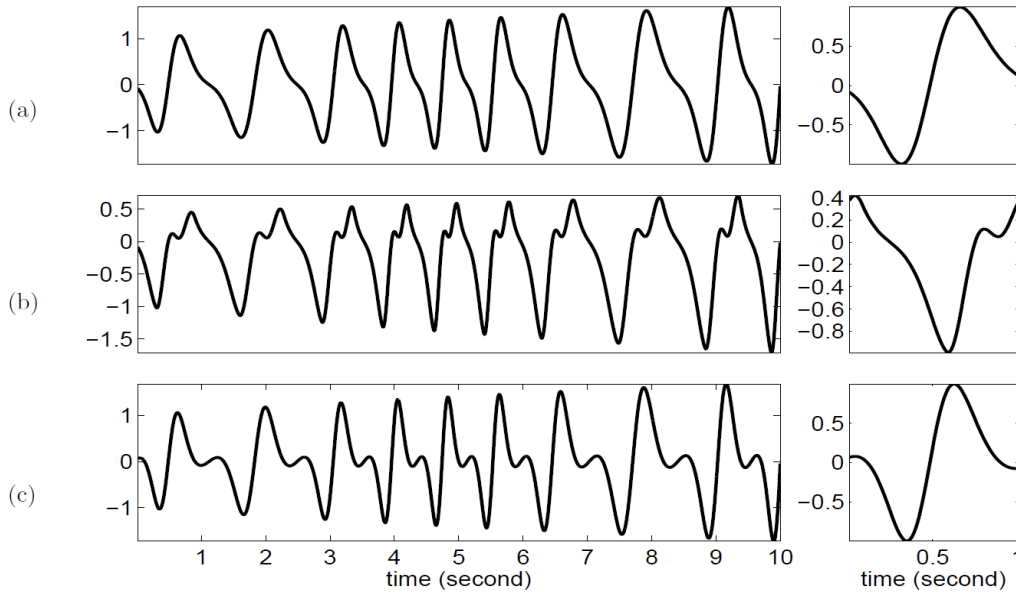


Figure 1: Toy examples of the type $f(t) = A(t)s(2\pi\phi(t))$. The amplitude modulation function and the phase function are identical for the three cases: $A(t) = \sqrt{1 + 0.2t}$ and $\phi(t) = t + 0.3\cos(t)$. In (a) the shape function $s(t)$ is given by $s(t) = \left[\cos(0.8\cos(t)) - \frac{\sin(t)}{\cos(t)} \sin(0.8\cos(t)) \right] \cos(t)$; in (b): $s(t) = \left[\cos(0.8\cos(t)) - \frac{\sin(t)}{\cos(t)} \sin(0.8\cos(t)) - 1.4\cos_+(t + 1/6)^2 \right] \cos(t)$; in (c): $s(t) = \left[\cos(1.2\cos(t)) - \frac{\sin(t)}{\cos(t)} \sin(1.2\cos(t)) \right] \cos(t)$.

\mathbb{R}^3 [9]; the recorded ECG signal is then viewed as the orthogonal projection of this dipole vector onto a fixed axis.¹ The ECG signal, recording the dynamics of the electrical activity of the heart, is a collection of periodic oscillating time series, one per channel, each corresponding to an ECG lead [7, 6]. The *waveforms* provide a lot of information about the anatomic or electrophysiological structure of the heart, essential in ascertaining certain medical conditions, such as ischemia or atrial fibrillation. On the other hand, the *variation of the time intervals between sequential heart beats*, referred to as “heart rate variability” (HRV), has been shown in the past few decades to be related to more general physiological dynamical processes [10]. To understand these different types of dynamics of the physiological system via the recorded ECG signal, it thus is beneficial to separate the shape of the oscillation from the variability of the time intervals between sequential oscillatory waveforms.

In this section, the example ECG signals are recorded from a healthy 33-year-old male, with 12 bit resolution and a sampling rate of 1000Hz. We show in Figure 2 the lead I and lead II ECG signals, which we denote as $\text{ECG}_I(t)$ and $\text{ECG}_{II}(t)$, $t \in [0, T]$. In the figure, the black curve is the usual ECG signal; the peaks indicated by red circles are called the R peaks [6]. One type of variation from one cycle to the next in the ECG signal can be clearly tracked by the changing time intervals between consecutive R-peaks. In clinical practice, the “heart rate” is given by simply counting the number of beats during a minute, that is, the “mean rate” over a given time period. However, there is information hidden inside the HRV, beyond the mean rate, that we want to describe quantitatively. To access this, let us first introduce an intuitive definition of time-dependent instantaneous heart rate (IHR), as the inverse of the time interval between the two most recent successive heart beats. We refer to this quantity as the *intuitive instantaneous heart rate* (or *intuitive instantaneous frequency*) and denote it as $\text{IHR}_i(t)$, where the subscript i refers to the “intuitive” character of this definition. Denoting by t_k the location of the R-peak of the k -th heart beat, $k = 1, \dots, N$. IHR_i is

¹In fact, the situation is a bit more complex. In addition to the periodic motion for every heartbeat, the trajectory in \mathbb{R}^3 of the current dipole vector is deformed by other phenomena such as breathing. We shall ignore these effects here.

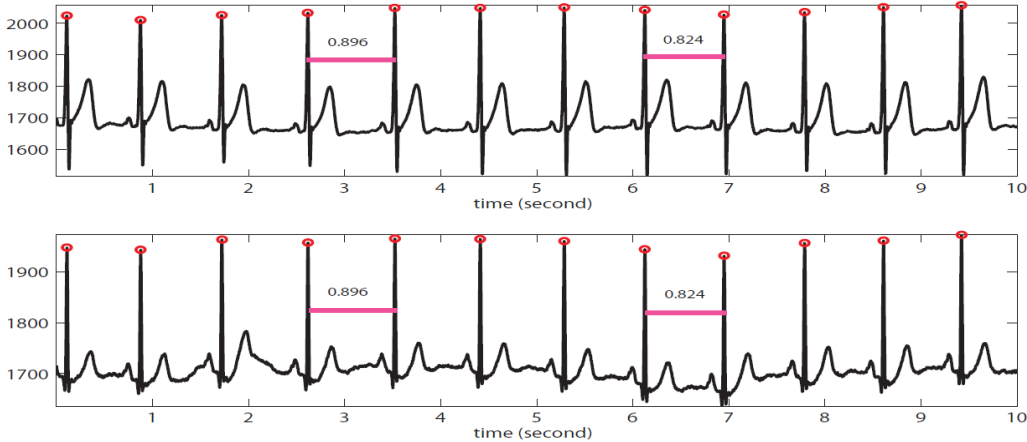


Figure 2: Top: the lead I ECG signal; bottom: the lead II ECG signal, where the red circles mark the locations of the R peaks. It is clear that the time interval between consecutive R-peaks is not constant.

defined as the piecewise constant function plotted in Figure 3,

$$\text{IHR}_i(t) = \frac{1}{t_k - t_{k-1}} \text{ if } t_k \leq t < t_{k+1}.$$

Note that the definition of IHR_i echoes the etymology of “frequency”: counting how *frequently* a phenomenon occurs per unit time.

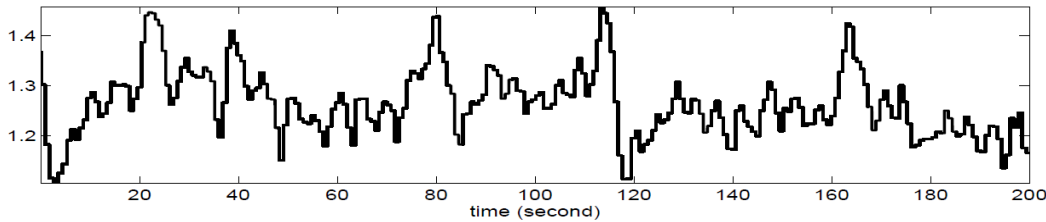


Figure 3: The intuitive instantaneous heart rate.

To a very good approximation, the ECG signals can be modeled as

$$\text{ECG}_\ell(t) = A_\ell(t)s_\ell(\phi_E(t)) + W_\ell(t),$$

where ℓ stands for the lead (or channel) number (e.g., I or II), and where $\phi_E(t)$ does not depend on ℓ . (The subscript E indicates that this is the $\phi(t)$ for the ECG signal; we shall meet other ϕ below.) The function $W_\ell(t)$ contains all the other components of the signal, including noise and low frequency baseline wandering. We show in this paper that the Synchrosqueezing transform can identify $\phi'_E(t)$ for signals of this type, with high accuracy, independently of the wave shape functions $s_\ell(t)$. Physiologically, the HRV reflects the periodic behavior of the current dipole vector; it should thus not depend on how we project this dipole vector. In other words, our estimate should be the same, whether we derive it from $\text{ECG}_\text{I}(t)$ or $\text{ECG}_\text{II}(t)$, i.e. whether the behavior in time of the wave shape function it modulates is associated with lead I or lead II. It turns out that the Synchrosqueezing estimate does indeed exhibit this invariance, as we demonstrate numerically here. (A mathematical explanation of this will be given in Section 3.) We denote the estimated ϕ'_E as $\text{IHR}_\ell(t)$ if it is estimated by computing the Synchrosqueezing transform of $\text{ECG}_\ell(t)$. Figures 4, resp. 5 plot $\text{IHR}_\text{I}(t)$, resp. $\text{IHR}_\text{II}(t)$ and shows that in both cases $\text{IHR}_\ell(t)$ is extremely close to IHR_i . In Figure 6,

IHR_I and IHR_{II} are plotted together, illustrating directly that our estimate of ϕ'_E does not depend on which wave shape function was being modulated. (That the two shape functions s_I and s_{II} are different is clear from Fig.2.) Furthermore, this example indicates that our estimate captures the “instantaneous frequency”: indeed, ϕ'_E matches IHR_i with high accuracy. This finding makes it possible to define an “instantaneous heart rate” for subjects with much less clearly defined heart beats: even if the $IHR_i(t)$ can no longer be defined because the t_k cannot be defined clearly, we can still estimate $IHR_\ell(t)$.

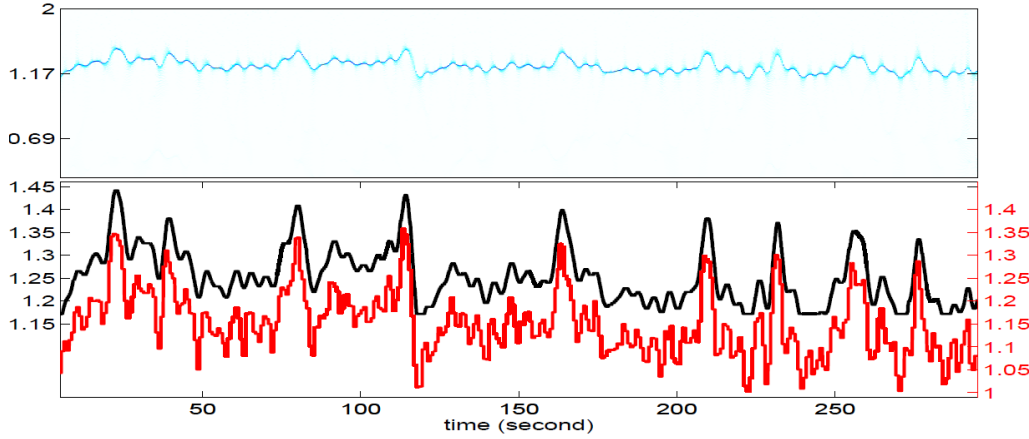


Figure 4: Top: the Synchrosqueezing transform of $ECG_I(t)$; bottom: the black curve is $IHR_I(t)$ estimated from the Synchrosqueezing transform of $ECG_I(t)$ and the red curve is $IHR_i(t)$ shifted down by 0.1.

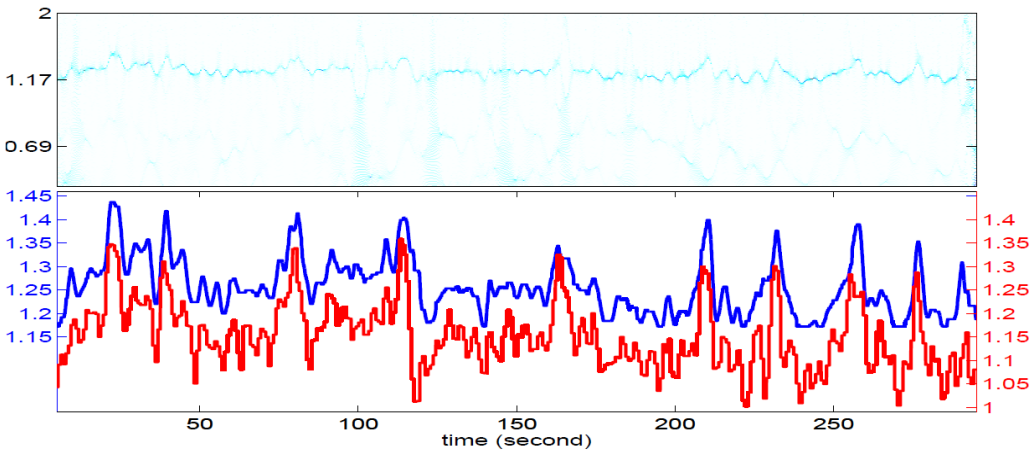


Figure 5: Top: the Synchrosqueezing transform of $ECG_{II}(t)$; bottom: the blue curve is $IHR_{II}(t)$ estimated from the Synchrosqueezing transform of $ECG_{II}(t)$ and the red curve is $IHR_i(t)$ shifted down by 0.1.

Our second example concerns the respiratory signal, i.e., the signal provided by a mechanical recording of the breathing process. Physiologically, the morphology of the recorded respiratory signal reflects the anatomical structure of our respiratory system [7]. In a first approximation, breathing is a periodic process; a closer look reveals that consecutive “breathing peaks” are not quite equally spaced (see Figure 7 below). This breathing rate variability (BRV) reflects the physiological dynamics [2, 14]. An example of a respiratory signal $Resp(t)$ is shown in Figure 7. The signal was recorded from a 28-year-old healthy male, with a sampling rate of 20 Hz. Like the ECG signal, to a very good approximation, the respiratory signal can be modeled as

$$Resp(t) = A(t)s(\phi_R(t)) + W(t),$$

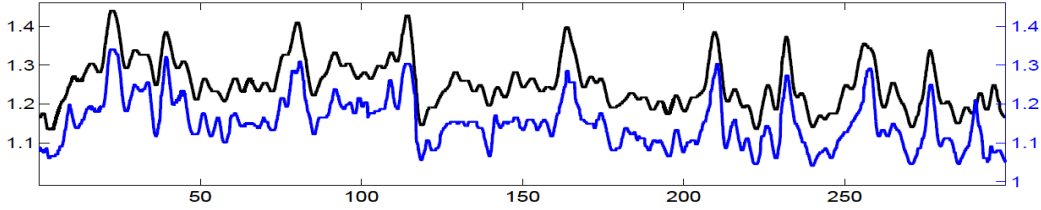


Figure 6: The blue curve is $IHR_I(t)$ and the black curve is $IHR_{II}(t)$ shifted down by 0.1.

where the subscript R indicates that this is the phase function $\phi(t)$ for the *respiratory* signal; the function $W(t)$ contains again all the other components of the signal, including noise and low frequency baseline wandering.

As in the discussion of the ECG signal, we first define an intuitive notion of time-dependent instantaneous breathing rate $IRR_i(t)$ as the inverse of the time interval between the two most recent successive breathing cycles. A breathing cycle is defined to be the signal between two consecutive ends of the inspiration; these ends are marked as the red circles in Figure 7. More precisely, we denote the location of the ends of the inspiration by t_i , $i = 1, \dots, M$ and define $IRR_i(t)$ as follows:

$$IRR_i(t) = \frac{1}{t_k - t_{k-1}} \text{ when } t_k \leq t < t_{k+1}.$$

The $IRR_i(t)$ is plotted as the black piecewise constant curve in Figure 7. Next, we apply the Synchrosqueezing transform directly on $Resp(t)$ and get an estimation of its instantaneous frequency, denoted by $IRR(t)$. In Figure 7, the $IRR(t)$ is superimposed on $Resp(t)$ and $IRR_i(t)$ to demonstrate that the estimated $IRR(t)$ captures the notion of instantaneous frequency. Indeed, the spacing of respiration cycles in $Resp(t)$ is reflected by $IRR(t)$: closer spacing corresponds to higher $IRR(t)$ values, and wider spacing to lower $IRR(t)$ values. In Figure 8 $IRR(t)$ and $IRR_i(t)$ are put together for comparison; they are clearly closely related.

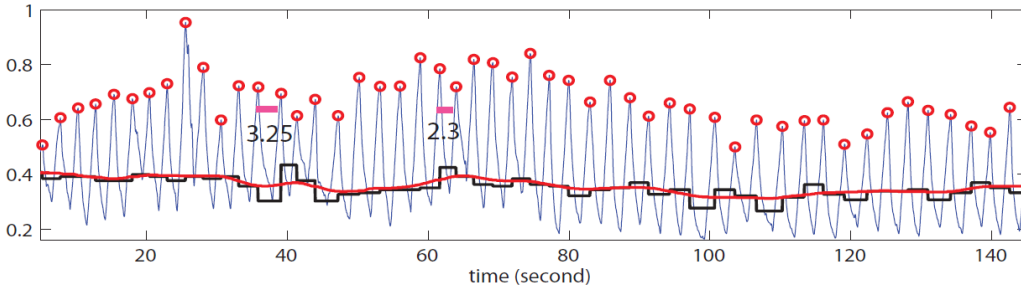


Figure 7: The blue curve is the respiratory signal $Resp(t)$; the black piecewise curve is the intuitive respiration rate $IRR_i(t)$.

For the sake of convenience, we shall use the acronym SST-IF for the *SynchroSqueezing Transform-derived Instantaneous Frequency* in what follows. Figure 9 shows a different breathing signal, and illustrates a direct physiological application of the respiration SST-IF. Sleep is a universally recurring physiological dynamical process. It is divided into two broad stages: rapid eye movement (REM) and non-rapid eye movement (NREM). Normally, sleep proceeds in cycles, each alternating between REM and NREM, with one cycle taking about 90 minutes. A clinically acceptable staging of the sleep is determined by reading the recorded electroencephalography (EEG) based on the R&K criteria, which were standardized in 1968 by Allan Rechtschaffen and Anthony Kales [12]. We take the staging according to this criteria as the gold standard, and we demonstrate that the respiration SST-IF can recover the gold standard staging of REM versus non-REM. The result is illustrated in Figure 9 which shows the SST-IF of a respiratory signal recorded

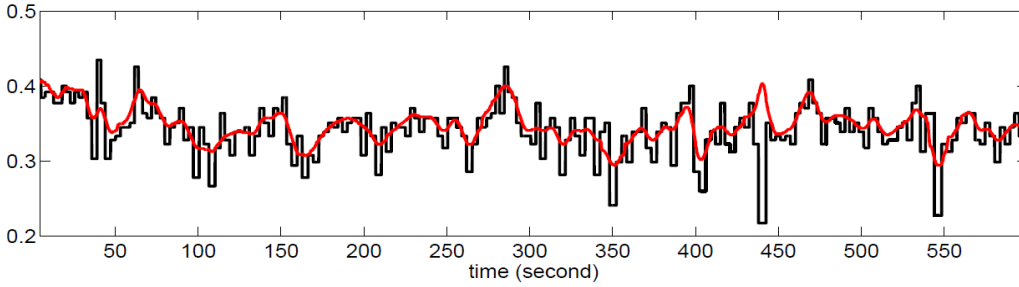


Figure 8: The red curve is the estimated instantaneous frequency $IRR(t)$ of the respiratory signal from the Synchrosqueezing transform, and the black piecewise curve is the intuitive respiration rate $IRR_i(t)$.

for about 8 hours with a 16 Hz sampling rate (original signal not shown here), and the corresponding sleep stages, denoted by $S(t)$, determined from a simultaneously recorded EEG according to the R&K criteria. High correlation is observed when comparing the time intervals with $S(t) = 5$ with SST-IF. ²

The discussion and examples in this Section illustrate the importance of an accurate determination of the “instantaneous frequency” of a signal, as captured by our SST-IF notion. In principle, we can determine instantaneous frequencies $\phi'(t)$ from representation of type (1) as well as from (2) or (4). We believe (and will argue in the next Section) that, at least for certain signals $f(t)$, modeling f as in (2) or (4), i.e., in terms of “wave shape functions” rather than with cosines, leads to more accurate estimates of the function $\phi'(t)$ via Synchrosqueezing, and probably also by other methods. For such signals, it is thus important to separate each component of f modeled as in (2) or (4) into a “wave shape function” on the one hand, and slowly varying amplitude and instantaneous frequency on the other hand.

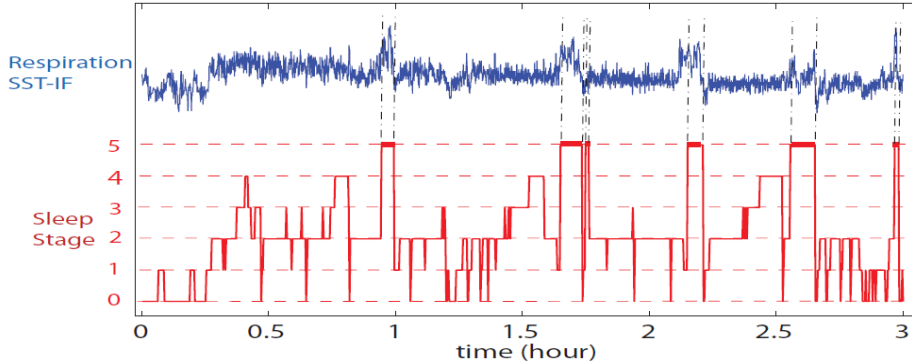


Figure 9: The blue curve is the $10 \times \text{SST-IF} + 4$, and the red piecewise function is the sleep stage determined from the simultaneously recorded EEG by the R&K criteria. The REM stage period is emphasized in both signals.

Another reason why it is important to separate “shape function” from “instantaneous frequency” is that the information hidden in the shape function is important in its own right, and can, for medical signals, be used for clinically quite different diagnoses. In other words, this separation allows us to tease apart two types of information that are commonly mixed-up. For example, reading ECG signals to diagnose cardiac disease in clinical practice amounts to evaluating the morphology of each heart beat, and this is given by the wave shape function. A well known example is the typical “ST elevation” in myocardial infarction patients.

²Further study and finding of the sleep cycle is beyond our scope here; a more detailed study will be presented in a later paper.

Another example is the qualitatively different spectral behavior of the morphology of the ECG shape function indicative of myocardial ischemia: the spectral analysis of ECG wave shape functions from dogs revealed a shift from high- to low-frequency ranges in ischemia cases [11]. Similar phenomena have been associated with balloon inflations during percutaneous transcatheter angioplasty in CAD patients [1]. We expect that a cleaner identification of the SST-IF will also lead to a separation of the shape function particularities with greater sensitivity, which in turn will be useful for clinical diagnoses linked to those particularities. A detailed discussion of this will have to wait for a subsequent paper; here we concentrate on the identification of the instantaneous frequency.

3. Theorem

We start by introducing some notations and conventions. As is customary, we say that τ is a period for the function $\varphi : \mathbb{R} \rightarrow \mathbb{C}$, or that φ is τ -periodic, if, for all $t \in \mathbb{R}$, and all $k \in \mathbb{Z}$, $\varphi(t + k\tau) = \varphi(t)$. We shall designate T to be *the* period for φ , if

$$\forall t \in \mathbb{R}, \forall k \in \mathbb{Z} : \varphi(t + kT) = \varphi(t) \text{ and } T = \inf(\{\tau; \tau > 0 \text{ and } \tau \text{ is a period for } \varphi\}) .$$

Next, we define a special class of wave shape functions that are dominated by one particular Fourier mode. More precisely,

Definition 3.1 (Shape function class $\mathcal{S}_{\mathbf{d}}^{\delta}$). The shape function class $\mathcal{S}_{\mathbf{d}}^{\delta}$ is the subset of $C^1(\mathbb{T})$ (the 2π -periodic continuously differentiable functions) consisting of functions s with bounded L^2 -norm for which all the Fourier modes \widehat{s}_k are dominated by the product of δ and the first mode coefficient, i.e.

$$\forall k \in \mathbb{Z}, \text{ with } k \neq 1, |\widehat{s}_k| \leq \delta |\widehat{s}_1| .$$

For example, $e^{i2\pi t}$ is a shape function, which is widely used in Fourier analysis. Indeed, $\widehat{e^{i2\pi t}}(n) = 1$ when $n = 1$ and 0 when $n \neq 1$ so that $e^{i2\pi t} \in \mathcal{S}_{\mathbf{d}}^0$. We demonstrate some examples in Figure 10: the shape function $s_{\text{II}}(t)$ for the ECG lead II signal satisfies $s_{\text{II}}(t) \in \mathcal{S}_{\mathbf{d}}^{3.4}$. (Note that the shape function $s_{\text{II}}(t)$ depends on the subject; different ECG signals may belong to different $\mathcal{S}_{\mathbf{d}}^{\delta}$; the value $\delta = 3.4$ is one of the larger we have encountered – more often δ can be picked closer to 1.)

Next, consider the following class of functions.

Definition 3.2 (Intrinsic Mode Functions class $\mathcal{C}_{\epsilon}^{\delta}$). For fixed choices of $\epsilon, \delta > 0$, $\epsilon \ll 1$, the space $\mathcal{C}_{\epsilon}^{\delta}$ of *Intrinsic Mode Functions (IMFs)* consists of functions $f \in C^{\infty}(\mathbb{R})$ having the form

$$f(t) = A(t)s(2\pi i\phi(t)), \tag{5}$$

where $s \in \mathcal{S}_{\mathbf{d}}^{\delta}$, such that A and ϕ satisfy the following conditions:

$$\begin{aligned} \forall m \geq 0, A^{(m)}, \phi^{(m)} &\in L^{\infty} \\ A(t) > 0, \phi'(t) > 0, \\ \|A'\|_{L^{\infty}} \leq \epsilon \|\phi'\|_{L^{\infty}}, \quad \|\phi''\|_{L^{\infty}} &\leq \epsilon \|\phi'\|_{L^{\infty}} . \end{aligned}$$

We then consider the function class $\mathcal{C}_{\epsilon, d}^{\delta}$, defined as follows.

Definition 3.3 (Superpositions of IMFs). The space $\mathcal{C}_{\epsilon, d}^{\delta}$ of *superpositions of IMFs* consists of functions f having the form

$$f(t) = \sum_{k=1}^K f_k(t)$$

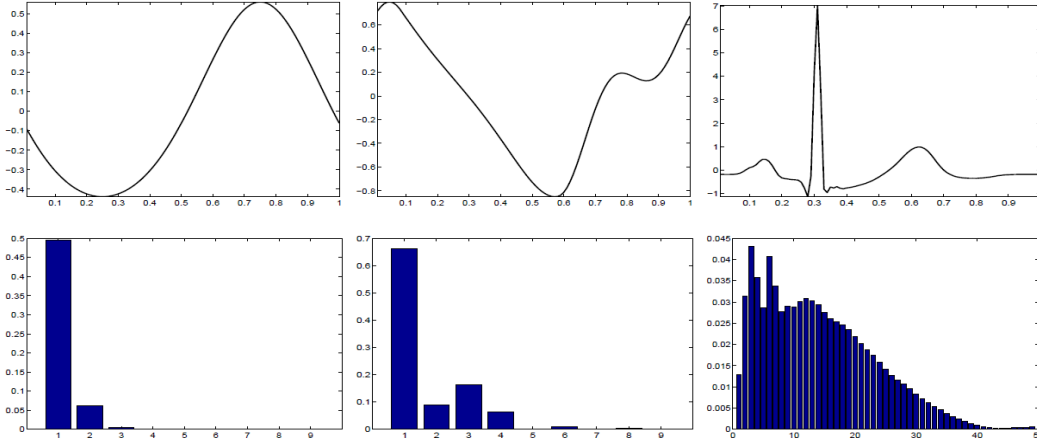


Figure 10: Three different shape functions $s_1(t)$, $s_2(t)$ and $s_{II}(t)$ (upper) and their spectrum (below). Left: $s_1(t)$ is equal to normalizing $\left[\cos(0.5 \cos(t)) - \frac{\sin(t)}{\cos(t)} \sin(0.5 \cos(t))\right] \cos(t)$ to be of unit L^2 norm; middle: $s_2(t)$ is equal to normalizing (3) to be of unit L^2 norm; right: s_{II} is a shape function for a particular lead II ECG signal.

for some $K > 0$ and $f_k = A_k s_k(2\pi i \phi_k) \in \mathcal{C}_\epsilon^\delta$ such that ϕ_k satisfy

$$\inf_t \phi'_k(t) - \sup_t \phi'_{k-1}(t) \geq d[\phi'_k(t) + \phi'_{k-1}(t)].$$

Note that $\mathcal{C}_{\epsilon,d}^\delta$ and \mathcal{S}_d^δ are not vector spaces; as in [4], the definition of $\mathcal{C}_{\epsilon,d}^\delta$ is also not the most general possible definition. We use this definition for the purpose of clarifying the main idea of this work. In the following, we denote $W_f(a,b)$ to be the continuous wavelet transform of $f \in L^\infty(\mathbb{R})$ with the mother wavelet ψ which is in the Schwartz space [3]. For simplicity, we shall assume $\text{supp} \widehat{\psi} \subset [1 - \Delta, 1 + \Delta]$, where $0 < \Delta \ll 1$; in practice, our results seem to hold under much less stringent conditions.

In the following we prove that the Synchrosqueezing transform discussed in [4] allows us to estimate the instantaneous frequency of each component of the functions in $\mathcal{C}_{\epsilon,d}^\delta$ with high accuracy when all the wave shape functions are close to the exponential function, i.e. when δ is sufficiently small. We also discuss the case when the function f itself is in $\mathcal{C}_\epsilon^\delta$, i.e. it has only one component; in this case the Synchrosqueezing transform still leads to an accurate estimate of the instantaneous frequency even if the wave shape function is quite different from the exponential $\exp(2\pi i \cdot)$, i.e. even for δ that are not small. Most of the estimates needed to prove these results follow Section 3 in [4]; we shall spell out the details only when care has to be taken with extra terms involving the possibly more complex shape of the wave shape functions.

Definition 3.4 (Instantaneous frequency information function). Let $f \in L^\infty(\mathbb{R})$. The *instantaneous frequency information function* of f is defined by

$$\omega_f(a,b) = \begin{cases} \frac{-i\partial_b W_f(a,b)}{W_f(a,b)} & |W_f(a,b)| > 0 \\ \infty & |W_f(a,b)| = 0 \end{cases}.$$

Note that this definition makes sense since $W_f(a,b) \in C^\infty(\mathbb{R}_+ \times \mathbb{R})$.

Remark. In practice, the determination of those (a,b) -pairs for which $W_f(a,b) = 0$ is rather unstable, when f has been contaminated by noise. For this reason, it is useful to consider a threshold for $|W_f(a,b)|$, below which $\omega(a,b)$ is not defined. The purpose of this function is to record the information of the instantaneous frequency, based on which the reassignment will be performed.

Then, we consider the following definition of the Synchrosqueezing based on the wavelet transform:

Definition 3.5 (Synchrosqueezing transform). For $f \in L^\infty(\mathbb{R})$, the *Synchrosqueezing transform with resolution* $\alpha > 0$ and *threshold* $\gamma \geq 0$ is defined by

$$S_f^{\alpha, \gamma}(b, \xi) := \int_{A_{\gamma, f}(b)} W_f(a, b) \frac{1}{\alpha} h\left(\frac{\xi - \omega_f(a, b)}{\alpha}\right) a^{-3/2} da, \quad (6)$$

where $A_{\gamma, f}(b) := \{a \in \mathbb{R}_+; |W_f(a, b)| > \gamma\}$, $h \in C_c^\infty$ with $\int h(t) dt = 1$.

Remark. Note that $\omega_f(a, b)$ and $S_f^{\alpha, \gamma}(b, \xi)$ can be defined for any L^∞ function f . However, when $f \in \mathcal{C}_{\epsilon, d}^\delta$, the next Theorem tells us that the Synchrosqueezing transform provides an accurate estimation of the instantaneous frequency and allows the reconstruction of each component.

Theorem 3.6. Let $f = \sum_{k=1}^K A_k(t) s_k(2\pi i \phi_k(t)) \in \mathcal{C}_{\epsilon, d}^\delta$ and suppose $\delta \leq \epsilon$. Set $\mathcal{R}_\psi = \sqrt{2\pi} \int \widehat{\psi}(z) z^{-1} dz$. Suppose $\Delta < d/(1+d)$. Denote $Z_k := \{(a, b) : |a\phi'_k(b) - 1| < \Delta\}$. Then, provided ϵ is sufficiently small, the following hold:

- $|W_f(a, b)| > \epsilon^{1/3}$ only when $(a, b) \in Z_k$ for some $k \in \{1, \dots, K\}$.
- For each pair $(a, b) \in Z_k$ for which $|W_f(a, b)| > \epsilon^{1/3}$, we have

$$|\omega_f(a, b) - \phi'_k(b)| \leq \epsilon^{1/3}.$$

- Moreover, for each $k \in \{1, \dots, K\}$ and all $b \in \mathbb{R}$,

$$\left| \lim_{\alpha \rightarrow 0} \left(\mathcal{R}_\psi^{-1} \int_{|\xi - \phi'_k(b)| < \gamma} S_f^{\alpha, \gamma}(b, \omega) d\xi \right) - A_k(b) \hat{s}_k(1) e^{i\phi_k(b)} \right| \leq C \epsilon^{1/3},$$

$$\text{where } C = 4 \left[\left(\frac{\phi'_k(b)}{1-\Delta} \right)^{1/2} - \left(\frac{\phi'_k(b)}{1+\Delta} \right)^{1/2} \right].$$

Because the proof of this Theorem is similar to the one carried out in [4, Theorem 3.3], except for some estimates, given in more detail below, we shall mostly only sketch the argument. In the statement and proof of all the Lemmas, we shall always assume that all the conditions of Theorem 3.6 are satisfied without repeating them, unless stated otherwise.

First of all, the ‘‘dyadic separation’’ condition in the definition of $\mathcal{C}_{\epsilon, d}^\delta$ implies that for every (a, b) –pair, at most one component of the signal ‘‘comes into play’’. The proof of the Lemma is the same as that of Estimate 3.6 in [4], so we omit it.

Lemma 3.7. For any pair (a, b) under consideration, there can be at most one $k \in \{1, \dots, K\}$ for which $|a\phi'_k(b) - 1| < \Delta$.

The following Lemma describes the result of applying the continuous wavelet transform to $f \in \mathcal{C}_{\epsilon, d}^\delta$. It is similar to Estimate 3.5 in [4] except for some extra terms due to the more general form of the wave shape functions; when $s_k(t) = e^{it}$ for all $k \in \{1, \dots, K\}$, we recover the statement and proof of Estimate 3.5 in [4].

Lemma 3.8. For $l \in \{1, \dots, K\}$ and $(a, b) \in Z_l$, we have

$$\left| W_f(a, b) - A_l(b) \hat{s}_l(1) e^{i2\pi\phi_l(b)} \sqrt{a} \widehat{\psi}(a\phi'_l(b)) \right| \leq \epsilon a^{1/2} \Gamma_1(a, b),$$

where

$$\Gamma_1(a, b) = \sum_{k=1}^K \left\{ a \|\phi'_k\|_\infty \|s_k\|_\infty m_1 + a^2 A_k(b) \|\phi'_k\|_\infty \|s'_k\|_\infty m_2 + m_0 \sum_{k=1}^K A_k(b) \left(\sum_{n \in \mathbb{N}, n \geq 2} \frac{|\hat{s}_k(n) \widehat{\psi}(a\phi'_k(b)n)|}{\epsilon} \right) \right\}$$

and $m_i = \int_{\mathbb{R}} |x|^i |\psi(x)| dx$.

Remark. Take $f = \sum_{k=1}^K f_k \in \mathcal{C}_{\epsilon,d}$ and fix f_l for some $l \in \{1, \dots, K\}$. We observe from this Lemma that the larger the l is, the larger the $\Gamma_1(a, b)$ in Lemma 3.8. Indeed, on the one hand, the larger l is, the more ϕ'_k will be smaller than ϕ'_l so that more $\hat{\psi}(a\phi'_k(b)n)$, $n > 1$ become positive. Consider a such that $a\phi'_l(b) \in [1 - \Delta, 1 + \Delta]$. For $k \in \{1, \dots, K\}$, $k < l$, $\hat{\psi}(a\phi'_k(b)n) \neq 0$ holds only if $\frac{n\phi'_k(b)(1-\Delta)}{\phi'_l(b)} < 1 + \Delta$ or $1 - \Delta < \frac{n\phi'_k(b)(1+\Delta)}{\phi'_l(b)}$, or equivalently

$$\frac{1 - \Delta}{1 + \Delta} \frac{\phi'_l(b)}{\phi'_k(b)} < n < \frac{1 + \Delta}{1 - \Delta} \frac{\phi'_l(b)}{\phi'_k(b)}. \quad (7)$$

Clearly when the l is large, $\hat{\psi}(a\phi'_k(b)n) \neq 0$ for more combinations of k and n . On the other hand, if $s_k(t) \neq e^{it}$ for some $k < l$, due to the existence of the nonzero high Fourier modes of the shape function $s_k(t)$, that is, $\hat{s}_k(n) \neq 0$ for $n > 1$, the nonzero $\hat{\psi}(a\phi'_k(b)n)$ will survive for those n for which $\hat{s}_k(n) \neq 0$. Thus, the continuous wavelet coefficients around Z_l will be ‘‘contaminated’’. Putting these two effects together, we expect that the larger l is and the larger the $\hat{s}_k(n)$, $n > 1$ and $k < l$ are, the larger the $\Gamma_1(a, b)$ will be. Moreover, besides Z_l , other blurred bands on the time–frequency plane than Z_k , $k = 1, \dots, K$, will be generated, especially on the bands near the multiples of the main IF $\phi'_k(b)$, $k = 1, \dots, K$, which depend on the wave shape functions. It is for these reasons that we shall evaluate the IF from the *lowest* mode $\hat{s}_k(n)$ of the s_k . We shall illustrate this below, in examples.

Proof. Since $f \in \mathcal{C}_{\epsilon,d} \subset L^\infty(\mathbb{R})$ and the mother wavelet $\psi(t)$ is a Schwartz function, $W_f(a, b)$ is well defined. To get the result, we need three estimations. First evaluate the following integration for $k \in \{1, \dots, K\}$ and $(a, b) \in \mathbb{R}_+ \times \mathbb{R}$:

$$\begin{aligned} & \int_{\mathbb{R}} A_k(b) s_k \left(2\pi(\phi_k(b) - b\phi'_k(b)) + 2\pi\phi'_k(b)t \right) \frac{1}{\sqrt{a}} \psi \left(\frac{t-b}{a} \right) dt \\ &= A_k(b) \int_{\mathbb{R}} s_k \left(2\pi(\phi_k(b) - b\phi'_k(b)) + 2\pi x \right) \frac{1}{\sqrt{a}} \psi \left(\frac{x - b\phi'_k(b)}{a\phi'_k(b)} \right) \frac{1}{\phi'_k(b)} dx \\ &= A_k(b) \int_{\mathbb{R}} \sum_{n \in \mathbb{Z}} \hat{s}_k(n) \delta_n e^{i2\pi(\phi_k(b) - b\phi'_k(b))} \sqrt{a} \hat{\psi}(a\phi'_k(b)\xi) e^{i2\pi\phi'_k(b)\xi} d\xi \\ &= A_k(b) \hat{s}_k(1) e^{i2\pi\phi_k(b)} \sqrt{a} \hat{\psi}(a\phi'_k(b)) + \sum_{n \in \mathbb{N}, n \geq 2} A_k(b) \hat{s}_k(n) e^{i2\pi\phi_k(b)} \sqrt{a} \hat{\psi}(a\phi'_k(b)n), \end{aligned} \quad (8)$$

where the second equality comes from the Plancherel equality.

Next, since $s_k \in C^1(T)$, by applying Taylor’s expansion to $\phi_k(t)$ and $s_k(t)$, we can evaluate the error generated by replacing $s_k(2\pi\phi_k(t))$ by $s_k(2\pi(\phi_k(b) - b\phi'_k(b)) + 2\pi\phi'_k(b)t)$:

$$\begin{aligned} & \int_{\mathbb{R}} A_k(b) s_k(2\pi\phi_k(t)) \frac{1}{\sqrt{a}} \psi \left(\frac{t-b}{a} \right) dt \\ &= \int_{\mathbb{R}} A_k(b) s_k \left[2\pi \left(\phi_k(b) - b\phi'_k(b) + \phi'_k(b)t + \phi''_k(t') \frac{(t-b)^2}{2} \right) \right] \frac{1}{\sqrt{a}} \psi \left(\frac{t-b}{a} \right) dt \\ &= \int_{\mathbb{R}} A_k(b) \left[s_k(2\pi(\phi_k(b) - b\phi'_k(b)) + 2\pi\phi'_k(b)t) + 2\pi s'_k(\bar{t}) \phi''_k(t') \frac{(t-b)^2}{2} \right] \frac{1}{\sqrt{a}} \psi \left(\frac{t-b}{a} \right) dt \\ &= \int_{\mathbb{R}} A_k(b) s_k(2\pi(\phi_k(b) - b\phi'_k(b)) + 2\pi\phi'_k(b)t) \frac{1}{\sqrt{a}} \psi \left(\frac{t-b}{a} \right) dt \\ & \quad + \frac{A_k(b)}{2} \int_{\mathbb{R}} \phi''_k(t') s'_k(\bar{t}) \frac{1}{\sqrt{a}} \psi \left(\frac{t-b}{a} \right) (t-b)^2 dt \end{aligned} \quad (9)$$

where the first equality comes from applying Taylor’s expansion to $\phi_k(t)$, and the second equality comes from the mean value theorem.

Third, we approximate $W_f(a, b)$ by Taylor's expansion on $A_k(t)$:

$$\begin{aligned} W_f(a, b) &= \sum_{k=1}^K \int_{\mathbb{R}} A_k(t) s_k(2\pi\phi_k(t)) \frac{1}{\sqrt{a}} \psi\left(\frac{t-b}{a}\right) dt \\ &= \sum_{k=1}^K \int_{\mathbb{R}} A_k(b) s_k(2\pi\phi_k(t)) \frac{1}{\sqrt{a}} \psi\left(\frac{t-b}{a}\right) dt + \sum_{k=1}^K \int_{\mathbb{R}} A'_k(t'')(t-b) s_k(2\pi\phi_k(t)) \frac{1}{\sqrt{a}} \psi\left(\frac{t-b}{a}\right) dt. \end{aligned} \quad (10)$$

When $l \in \{1, \dots, K\}$ and $(a, b) \in \mathbb{R}_+ \times \mathbb{R}$ such that $|a\phi'_l(b) - 1| \leq \Delta$, (8)-(10) together lead to the result:

$$\begin{aligned} & |W_f(a, b) - A_l(b) \hat{s}_l(1) e^{i2\pi\phi_l(b)} \sqrt{a} \hat{\psi}(a\phi'_l(b))| \\ & \leq \left| \sum_{k=1, k \neq l}^K A_k(b) \hat{s}_k(1) e^{i2\pi\phi_k(b)} \sqrt{a} \hat{\psi}(a\phi'_k(b)) + \sum_{k=1}^K \sum_{n \in \mathbb{N}, n \geq 2} A_k(b) \hat{s}_k(n) e^{i2\pi\phi_k(b)} \sqrt{a} \hat{\psi}(a\phi'_k(b)n) \right| \\ & \quad + \sum_{k=1}^K \left| \int_{\mathbb{R}} A'_k(t'')(t-b) s_k(2\pi\phi_k(t)) \frac{1}{\sqrt{a}} \psi\left(\frac{t-b}{a}\right) dt \right| \\ & \quad + \sum_{k=1}^K \left| \frac{A_k(b)}{2} \int_{\mathbb{R}} \phi''_k(t') s'_k(\bar{t}) \frac{1}{\sqrt{a}} \psi\left(\frac{t-b}{a}\right) (t-b)^2 dt \right| \end{aligned} \quad (11)$$

By the definition of IMFs, the second term and the third term in (11) are bounded by $\epsilon (\sum_{k=1}^K \|\phi'_k\|_{\infty} \|s_k\|_{\infty} a^{3/2} m_1 + \sum_{k=1}^K A_k(b) \|\phi'_k\|_{\infty} \|s'_k\|_{\infty} a^{5/2} m_2)$. Moreover,

$$\sum_{k=1}^K \sum_{n \in \mathbb{N}, n \geq 2} A_k(b) \hat{s}_k(n) e^{i2\pi\phi_k(b)} \sqrt{a} \hat{\psi}(a\phi'_k(b)n) \leq a^{1/2} m_0 \sum_{k=1}^K A_k(b) \left(\sum_{n \in \mathbb{N}, n \geq 2} |\hat{s}_k(n) \hat{\psi}(a\phi'_k(b)n)| \right),$$

which finishes the proof. \square

In the next Lemma, we show that by differentiating the continuous wavelet transform, the instantaneous frequency $\phi'_k(b)$ pops out. Though the instantaneous frequency is mixed up with other quantities, we will show that, when handled properly, this gives us an estimate of the instantaneous frequency with high accuracy. This Lemma is analogous to Lemma 3.9 in [4].

Lemma 3.9. For $k \in \{1, \dots, K\}$ and $(a, b) \in Z_k$, we have

$$\left| -i\partial_b W_f(a, b) - 2\pi A_k(b) \hat{s}_k(1) e^{i2\pi\phi_k(b)} \phi'_k(b) \sqrt{a} \hat{\psi}(a\phi'_k(b)) \right| \leq \epsilon a^{1/2} \Gamma_2(a, b),$$

where

$$\Gamma_2(a, b) = \sum_{k=1}^K \left\{ \|\phi'_k\|_{\infty} \|s_k\|_{\infty} m'_1 + a A_k(b) \|\phi'_k\|_{\infty} \|s'_k\|_{\infty} m'_2 + 2\pi A_k(b) m_0 \left(\sum_{n \in \mathbb{N}, n \geq 2} \frac{|\hat{s}_k(n) \hat{\psi}(a\phi'_k(b)n)|}{\epsilon} \right) \right\}$$

and $m'_i = \int_{\mathbb{R}} |x|^i |\psi'(x)| dx$.

Proof. The proof follows the same lines as that for Lemma 3.8. Under the same conditions, we can evaluate the following approximations. First,

$$\int_{\mathbb{R}} A_k(b) s_k(2\pi(\phi_k(b) - b\phi'_k(b)) + 2\pi\phi'_k(b)t) \frac{1}{a^{3/2}} \psi'\left(\frac{t-b}{a}\right) dt \quad (12)$$

$$\begin{aligned}
&= A_k(b) \int_{\mathbb{R}} s_k(2\pi(\phi_k(b) - b\phi'_k(b)) + 2\pi x) \frac{1}{a^{3/2}} \psi' \left(\frac{x - b\phi'_k(b)}{a\phi'_k(b)} \right) \frac{1}{\phi'_k(b)} dx \\
&= A_k(b) \int_{\mathbb{R}} \sum_{n \in \mathbb{Z}} \hat{s}_k(n) \delta_n e^{i2\pi(\phi_k(b) - b\phi'_k(b))} i2\pi\phi'_k(b) \sqrt{a} \hat{\psi}(a\phi'_k(b)\xi) e^{i2\pi\phi'_k(b)} d\xi \\
&= i2\pi A_k(b) \hat{s}_k(1) \phi'_k(b) e^{i2\pi\phi_k(b)} \sqrt{a} \hat{\psi}(a\phi'_k(b)) + i2\pi A_k(b) \phi'_k(b) \sum_{n \in \mathbb{N}, n \geq 2} \hat{s}_k(n) e^{i2\pi\phi_k(b)} \sqrt{a} \hat{\psi}(a\phi'_k(b)n).
\end{aligned}$$

Second,

$$\begin{aligned}
&\int_{\mathbb{R}} A_k(b) s_k(2\pi\phi_k(t)) \frac{1}{a^{3/2}} \psi' \left(\frac{t-b}{a} \right) dt \tag{13} \\
&= \int_{\mathbb{R}} A_k(b) s_k \left[2\pi \left(\phi_k(b) - b\phi'_k(b) + \phi'_k(b)t + \phi''_k(t) \frac{(t-b)^2}{2} \right) \right] \frac{1}{a^{3/2}} \psi' \left(\frac{t-b}{a} \right) dt \\
&= \int_{\mathbb{R}} A_k(b) s_k(2\pi(\phi_k(b) - b\phi'_k(b)) + 2\pi\phi'_k(b)t) \frac{1}{a^{3/2}} \psi' \left(\frac{t-b}{a} \right) dt \\
&\quad + \frac{A_k(b)}{2} \int_{\mathbb{R}} \phi''_k(t) s'_k(\bar{t}) \frac{1}{a^{3/2}} \psi' \left(\frac{t-b}{a} \right) (t-b)^2 dt;
\end{aligned}$$

and third,

$$\begin{aligned}
W_f(a, b) &= \sum_{k=1}^K \int_{\mathbb{R}} A_k(t) s_k(2\pi\phi_k(t)) \frac{1}{a^{3/2}} \psi' \left(\frac{t-b}{a} \right) dt \tag{14} \\
&= \sum_{k=1}^K A_k(b) \int_{\mathbb{R}} s_k(2\pi\phi_k(t)) \frac{1}{a^{3/2}} \psi' \left(\frac{t-b}{a} \right) dt + \sum_{k=1}^K \int_{\mathbb{R}} A'_k(t'')(t-b) s_k(2\pi\phi_k(t)) \frac{1}{a^{3/2}} \psi' \left(\frac{t-b}{a} \right) dt.
\end{aligned}$$

By the same argument as that for Lemma 3.8, (12)-(14) together lead to the result:

$$\begin{aligned}
&| -i\partial_b W_f(a, b) - 2\pi A(b) \hat{s}(1) e^{i2\pi\phi(b)} \phi'(b) \sqrt{a} \hat{\psi}(a\phi'(b)) | \\
&\leq 2\pi \left| \sum_{k=1, k \neq l}^K A_k(b) \hat{s}_k(1) e^{i2\pi\phi_k(b)} \sqrt{a} \hat{\psi}(a\phi'_k(b)) + \sum_{k=1}^K A_k(b) \phi'_k(b) \sum_{n \in \mathbb{N}, n \geq 2} \hat{s}_k(n) e^{i2\pi\phi_k(b)} \sqrt{a} \hat{\psi}(a\phi'_k(b)n) \right| \\
&\quad + \sum_{k=1}^K \left| \int_{\mathbb{R}} A'_k(t'')(t-b) s_k(2\pi\phi_k(t)) \frac{1}{a^{3/2}} \psi' \left(\frac{t-b}{a} \right) dt \right| \\
&\quad + \sum_{k=1}^K \left| \frac{A_k(b)}{2} \int_{\mathbb{R}} \phi''_k(t) s'_k(\bar{t}) \frac{1}{a^{3/2}} \psi' \left(\frac{t-b}{a} \right) (t-b)^2 dt \right| \\
&\leq \epsilon a^{1/2} \sum_{k=1}^K \left\{ \|\phi'_k\|_{\infty} \|s_k\|_{\infty} m'_1 + a A_k(b) \|\phi'_k\|_{\infty} \|s'_k\|_{\infty} m'_2 + 2\pi A_k(b) m_0 \left(\sum_{n \in \mathbb{N}, n \geq 2} \frac{|\hat{s}_k(n) \hat{\psi}(a\phi'_k(b)n)|}{\epsilon} \right) \right\},
\end{aligned}$$

where the last inequality holds by the same argument as in (11) in Lemma 3.8. \square

The same remark for Lemma 3.8 holds for Lemma 3.9. That is, the larger the difference between the wave shape functions and the cosine function, the larger the possible negative effect on the precision of the estimate. The following Lemma clarifies the role of the function $\omega_f(a, b)$. Indeed it says that $\omega_f(a, b)$ provides the information of the instantaneous frequency of each component. Since the proof of this Lemma is the same as that of Estimate 3.8 in [4], we shall skip it.

Lemma 3.10. For $k \in \{1, \dots, K\}$, and $(a, b) \in Z_k$. Suppose $|W_f(a, b)| \geq \epsilon^{1/3}$, we have

$$|\omega_f(a, b) - \phi'_k(b)| \leq \epsilon^{2/3} a^{1/2} (\Gamma_1 \phi'_k(b) + \Gamma_2).$$

It is now clear that with appropriate restrictions on ϵ , the first two claims in the Theorem are proved. Note that the uniform lower and upper bounds on $\phi'_k(b)$ imply that the values of a for which $(a, b) \in Z_k$, for some $k \in \{1, \dots, K\}$, are uniformly bounded. It then follows that $\Gamma_1(a, b)$ is uniformly bounded as well. For $(a, b) \in \cup_{k=1}^K Z_k$, if we impose

$$\epsilon < a^{-3/4} \Gamma_1^{-3/2}(a, b), \quad (15)$$

then $\epsilon a^{1/2} \Gamma_1(a, b) < \epsilon^{1/3}$. If further we impose the condition that

$$\epsilon < a^{-3/2} (\Gamma_1 \phi'_k(b) + \Gamma_2)^{-3}, \quad (16)$$

then $\epsilon^{2/3} a^{1/2} (\Gamma_1 \phi'_k(b) + \Gamma_2) < \epsilon^{1/3}$.

The final Lemma concerns the reconstruction of each component; when $s_k(t) = e^{it}$ for all $k = 1, \dots, K$, we recover Lemma 3.9 in [4]. The proof of this Lemma is the same as that of Estimate 3.9 in [4], and we skip it. Notice that the error constant C does not depend explicitly on the wave shape functions; the dependence is hidden in (15) and (16).

Lemma 3.11. Suppose that both (15) and (16) are satisfied, and that, in addition, for all b and $k \in \{1, \dots, K\}$ under consideration,

$$\epsilon \leq 1/8d^3 [\phi'_1(b) + \phi'_2(b)]^3. \quad (17)$$

Then for any $b \in \mathbb{R}$

$$\left| \lim_{\alpha \rightarrow 0} \left(\mathcal{R}_\psi^{-1} \int_{|\xi - \phi'_k(b)| < \epsilon^{1/3}} S_f^{\alpha, \epsilon^{1/3}}(b, \xi) d\xi \right) - A_k(b) \hat{s}_k(1) e^{i2\pi \phi_k(b)} \right| \leq C \epsilon^{1/3},$$

where $C = 4 \left[\left(\frac{\phi'_k(b)}{1-\Delta} \right)^{1/2} - \left(\frac{\phi'_k(b)}{1+\Delta} \right)^{1/2} \right]$.

Combining Lemmas 3.8-3.11 completes the proof of Theorem 3.6.

Remark. This Theorem suggests that if we know a priori that the components of the signal have wave shape function close to an imaginary exponential (or if its real part has components close to a cosine function), then focusing on the band around the instantaneous frequency $\phi'_k(b)$ allows us to partially recover the signal. It is a partial recovery only since the information of the wave shape function $s_k(t)$ is not recovered here.

Next we consider the special case when the signal consists of only one component in $\mathcal{C}_\epsilon^\delta$. (Note that the ECG signal and the respiration signal are both signals of this kind.) In this special case, the Synchrosqueezing transform works well on more general shape functions, that is, we can remove the $\delta \leq \epsilon$ condition in Theorem 3.6. The proof is essentially the same as for Theorem 3.6.

Theorem 3.12. Let $f(t) = A(t)s(2\pi\phi(t)) \in \mathcal{C}_\epsilon^\delta$, $\delta > 0$. Set $\mathcal{R}_\psi = \sqrt{2\pi} \int \widehat{\psi}(z) z^{-1} dz$. Denote $Z := \{(a, b) : |a\phi'(b) - 1| < \Delta\}$. Then, provided ϵ is sufficiently small, the following hold:

- $|W_f(a, b)| > \epsilon^{1/3}$ only when $(a, b) \in Z$.
- For each pair $(a, b) \in Z$ for which $|W_f(a, b)| > \epsilon^{1/3}$, we have

$$|\omega_f(a, b) - \phi'(b)| \leq \epsilon^{1/3}.$$

- Moreover, for all $b \in \mathbb{R}$,

$$\left| \lim_{\alpha \rightarrow 0} \left(\mathcal{R}_\psi^{-1} \int_{|\xi - \phi'(b)| < \gamma} S_f^{\alpha, \gamma}(b, \omega) d\xi \right) - A(b) \hat{s}(1) e^{i\phi(b)} \right| \leq C \epsilon^{1/3},$$

$$\text{where } C = 4 \left[\left(\frac{\phi'(b)}{1-\Delta} \right)^{1/2} - \left(\frac{\phi'(b)}{1+\Delta} \right)^{1/2} \right].$$

We mention that in practice, we expect δ to be close to 1. For example, the wave shape function s_{II} of the ECG signal in Figure 10 is in $\mathcal{S}_{\mathbf{q}}^\delta$, with $\delta = 3.4$.

Now we demonstrate some numerical results of applying the Synchrosqueezing transform to analyze the functions in $\mathcal{C}_{\epsilon, d}^\delta$. Take the phase functions $\phi_L(t) = 1.5t + 0.2 \cos(t + 1)$ and $\phi_H(t) = 4.5(t + 0.2 \cos(t))$ and the amplitude modulation functions $A_L(t) = 1 + 0.1 \sin(t^{1.1})$ and $A_H(t) = \sqrt{1 + \cos(t)}$. Consider the following two functions for comparison:

$$f_1(t) = A_L(t) s_{\text{II}}(2\pi\phi_L(t)) + A(t) s_1(2\pi\phi_H(t))$$

and

$$f_2(t) = \frac{A_L(t)}{3.5} \cos(2\pi\phi_L(t)) + A(t) s_1(2\pi\phi_H(t)),$$

where $s_1(t)$ and $s_{\text{II}}(t)$ are the shape functions demonstrated in Figure 10. Clearly, f_1 and f_2 are both composed of one component with instantaneous frequency $1 - 0.2 \sin(t+1)$ and one component with instantaneous frequency $4 - 0.8 \sin(t)$ but with different wave shape functions in the low frequency component.

As is shown in Figure 10, the coefficients of the high Fourier modes of s_{II} are quite significant, whereas those of $\frac{1}{3.5} \cos(t)$ are all 0. In this case, since ϕ_H is roughly 3 times ϕ_L , it is the coefficient of the third Fourier mode of s_{II} that matters. Thus, according to Theorem 3.6, we expect to have worse ϕ'_H estimation from f_1 , which is borne out by Figure 11.

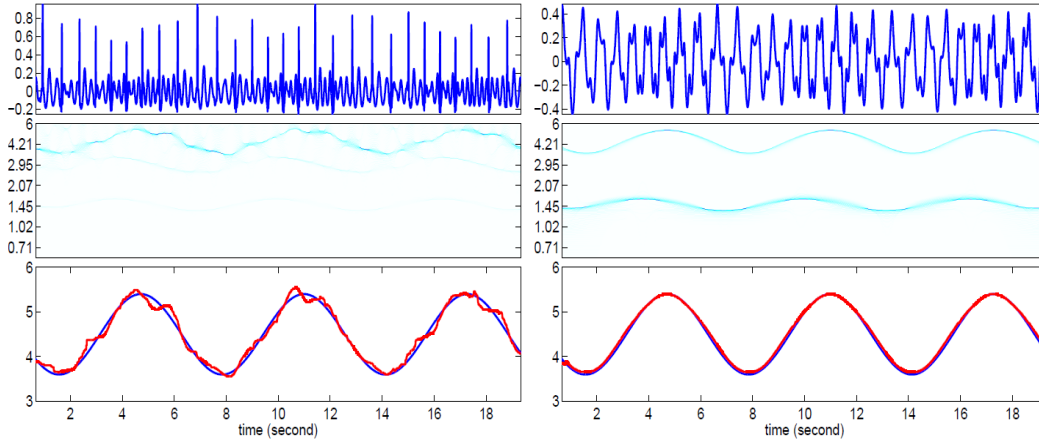


Figure 11: Left top: the f_1 signal; left middle: the Synchrosqueezing transform of f_1 , where the y-axis is demonstrated in the log scale; left bottom: the blue curve is $\phi'_L(t)$, while the red curve is the estimated ϕ'_H ; right top: the f_2 signal; right middle: the Synchrosqueezing transform of f_2 , where the y-axis is demonstrated in the log scale; right bottom: the blue curve is $\phi'_L(t)$, while the red curve is the estimated ϕ'_H . It is clear that the estimation of ϕ'_H is worse in f_1 . Notice that the dominant curve around ϕ'_L in the left middle figure is not very marked. This is caused by the small coefficient of the first Fourier mode of \hat{s}_{II} .

Next we show that if there is only one component in the function inside $\mathcal{C}_{\epsilon, d}^\delta$, that is, $f(t) = A(t) s(2\pi\phi(t))$, then according the Theorem 3.12, the dominant curve in the lowest part of the time frequency plane determined by the Synchrosqueezing transform provides an accurate estimation of the $\phi'(t)$. Take s_{II} shown in

Figure 10, $\phi(t) = 3(t + 0.2 \cos(t))$ and $A(t) = \sqrt{1 + 0.2 \cos(t)}$, that is,

$$f_{\text{II}}(t) = A(t)s_{\text{II}}(2\pi\phi(t)).$$

Since the coefficients of the high Fourier mode of s_{II} is dominant compared with the first Fourier mode, as is shown in Figure 10, the dominant curve in the lowest part of the time frequency plane is relatively less marked than the other dominant curves above it, but it leads to a more precise estimate of the instantaneous frequency, as shown in Figure 12.

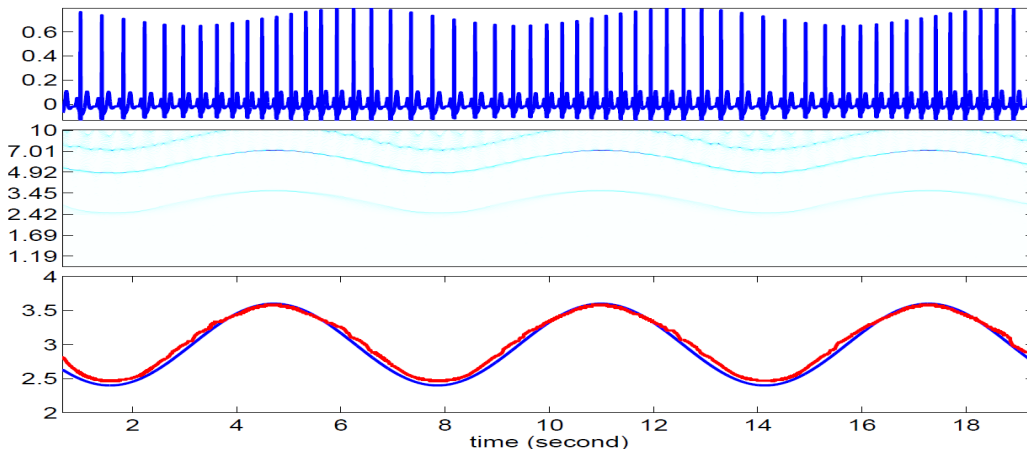


Figure 12: Top: the f_{II} signal; middle: the Synchrosqueezing transform of f_{II} , where the y-axis is demonstrated in the log scale; bottom: the blue curve is $\phi'(t) = 3 - 0.6 \sin(t)$, while the red curve is the estimated ϕ' . Notice that the estimation of $\phi'(t)$ is deteriorated by the existence of large coefficients of the high Fourier modes of \hat{s}_{II} .

4. Acknowledgements

The author acknowledges support by FHWA grant DTFH61-08-C-00028; he is also grateful for valuable discussions with Eugene Brevdo, Gaurav Thakur and Professor Ingrid Daubechies, and to Professor Chung-Kang Peng for kindly providing the respiratory signal during sleep and for many discussions.

References

- [1] S. Abboud, R.J. Cohen, A. Selwyn, P. Ganz, D. Sadeh, and P.L. Friedman, *Detection of transient myocardial ischemia by computer analysis of standard and signal-averaged high-frequency electrocardiograms in patients undergoing percutaneous transluminal coronary angioplasty*, *Circulation* **76** (1987), 585–596.
- [2] G. Benchetrit, *Breathing pattern in humans: diversity and individuality*, *Respiration Physiology* **122** (2000), no. 2-3, 123 – 129.
- [3] I. Daubechies, *Ten lectures on wavelets*, SIAM, 1992.
- [4] I. Daubechies, J. Lu, and H.-T. Wu, *Synchrosqueezed wavelet transforms: An empirical mode decomposition-like tool*, *Applied and Computational Harmonic Analysis* (2010).
- [5] I. Daubechies and S. Maes, *A nonlinear squeezing of the continuous wavelet transform based on auditory nerve models*, *Wavelets in Medicine and Biology* (1996), 527–546.

- [6] A. L. Goldberger, *Clinical electrocardiography: A simplified approach*, Mosby, 2006.
- [7] A. Guyton and J. Hall, *Textbook of medical physiology*, Saunders, 2000.
- [8] N. E. Huang, Z. Wu, S. R. Long, K. C. Arnold, K. Blank, and T. W. Liu, *On instantaneous frequency*, *Advances in Adaptive Data Analysis* **1** (2009), 177–229.
- [9] J. Keener, *Mathematical physiology*, Springer, 1998.
- [10] M. Malik and A. J. Camm, *Heart rate variability*, Wiley-Blackwell, 1995.
- [11] V. Mor-Avi and S. Akselrod, *Spectral analysis of canine epicardialelectrogram. short-term variations in the frequency content induced by myocardial ischemia*, *Circulation Research* **66** (1990), 1681–1691.
- [12] A. Rechtschaffen and A. Kales, *A manual of standardized terminology, techniques and scoring system for sleep stages of human subjects*, Washington: Public Health Service, US Government Printing Office, 1968.
- [13] G. Thakur and H.T. Wu, *Synchrosqueezing-based Recovery of Instantaneous Frequency from Nonuniform Samples*, Submitted (Arxiv preprint arXiv:1006.2533) (2010).
- [14] M. Wysocki, C. Cracco, A. Teixeira, A. Mercat, J. Diehl, Y. Lefort, J Derenne, and T Similowski, *Reduced breathing variability as a predictor of unsuccessful patient separation from mechanical ventilation*, *Critical Care Medicine* **34** (2006), 2076–2083.